

University of Texas Rio Grande Valley

ScholarWorks @ UTRGV

Theses and Dissertations

8-2021

Bioprinting a 3D Tubular Structure with Vascular Smooth Muscle Cells to Observe the Process Compatibility

Taieba Tuba Rahman

The University of Texas Rio Grande Valley

Follow this and additional works at: <https://scholarworks.utrgv.edu/etd>



Part of the [Manufacturing Commons](#)

Recommended Citation

Rahman, Taieba Tuba, "Bioprinting a 3D Tubular Structure with Vascular Smooth Muscle Cells to Observe the Process Compatibility" (2021). *Theses and Dissertations*. 944.

<https://scholarworks.utrgv.edu/etd/944>

This Thesis is brought to you for free and open access by ScholarWorks @ UTRGV. It has been accepted for inclusion in Theses and Dissertations by an authorized administrator of ScholarWorks @ UTRGV. For more information, please contact justin.white@utrgv.edu, william.flores01@utrgv.edu.

BIOPRINTING A 3D TUBULAR STRUCTURE WITH VASCULAR SMOOTH MUSCLE
CELLS TO OBSERVE THE PROCESS COMPATIBILITY

A Thesis

by

TAIEBA TUBA RAHMAN

Submitted to the Graduate College of
The University of Texas Rio Grande Valley
In partial fulfillment of the requirements for the degree of

MASTER OF SCIENCE IN ENGINEERING

August 2021

Major Subject: Manufacturing Engineering

BIOPRINTING A 3D TUBULAR STRUCTURE WITH VASCULAR SMOOTH MUSCLE
CELLS TO OBSERVE THE PROCESS COMPATIBILITY

A Thesis
by
Taieba Tuba Rahman

COMMITTEE MEMBERS

Dr. Jianzhi Li
Chair of Committee

Dr. Douglas Timmer
Committee Member

Dr. Farid Ahmed
Committee Member

Dr. Andrew Tsin
Committee Member

Dr. Xiaoqian Fang
Committee Member

August 2021

Copyright 2021 Taieba Tuba Rahman

All Rights Reserved

ABSTRACT

Rahman, Taieba T., Bioprinting a 3D Tubular Structure with Vascular Smooth Muscle Cells to Observe the Process Compatibility. Master of Science in Engineering (MSE), August, 2021, 41 pp, 14 tables, 20 figures, 34 references.

Printability is the ability to print a reproducible structure using the bioprinting technique. Constructing the relationships between printability and printing parameters of the extrusion printing process is difficult because of the presence of too many independent and inter-correlated factors. For this reason, it is necessary to identify and limit the number of significantly influential factors. In addition, Scaffold based blood vessel fabrication is a key challenge in 3D Bioprinting. As vascular smooth muscle cell (VSMCs) is a major component of blood vessels, the investigation of the behavior and orientation of VSMCs after printing is required to better understand the 3D bioprinting process of the blood vessel. This study fabricated a hollow tubular structure with human aortic smooth muscle cells using the co-axial extrusion printing method to observe the process compatibility. Response surface methodology (RSM) was used to find the optimum process parameters. The goal of this study was to ensure repeatable printing with the same dimension and consistency with these optimum process parameters. In the next phase, a cell-laden tubular structure was fabricated to observe the viability of vascular smooth muscle cells.

Keywords: VSMC; Co-axial extrusion printing; Hydrogels, RSM

DEDICATION

I dedicate my work to my mother “Saleha Begum”, my father “Md. Anisur Rahman”, and my husband “Mostafa Meraj Pasha”. I am thankful to my parents for their affection, advice, encouragement, and support all through my life. Finally, yet importantly, I would like to say a special thanks to my husband for his inspiration, support, and assistance during this journey.

ACKNOWLEDGMENTS

I would like to express my deep gratitude to my supervisor, Dr. Jianzhi Li, for his valuable guidance, suggestion, advice, and support throughout my master's study.

Most of the experiments in this dissertation were conducted in the Biomanufacturing Lab at the Biomedical Research Building, University of Texas Rio Grande Valley. I am grateful to have the privilege to work in this facility. I would particularly like to thank Victoria Perez, Reanna Rodriguez, Md Shakil Arman for their practical assistance on this research work

I want to thank Al Mazedur Rahman, Asma Akhter Mowshumi, Sharmin Emu, and Humayra Ava for making my journey smooth in UTRGV.

.

TABLE OF CONTENTS

	Page
ABSTRACT.....	iii
DEDICATION.....	iv
ACKNOWLEDGMENTS	v
TABLE OF CONTENTS.....	vi
LIST OF TABLES	viii
LIST OF FIGURES	ix
CHAPTER I.INTRODUCTION.....	1
CHAPTER II.LITERATURE REVIEW	4
CHAPTER III.METHODOLOGY	9
3.1 Bioink Preparation.....	9
3.2 Co-axial Extrusion Printing.....	10
3.3 Experiment Design.....	14
3.4 Cell Culturing.....	16
3.5 Cell Viability in proposed bioink	17
CHAPTER IV.RESULT AND DISCUSSION.....	18
4.1 Printability assessment with the different concentration of solutions.....	18
4.2 Printability assessment with the process parameter	24
4.3 3D printing with cell laden bioink.....	32

CHAPTER V.CONCLUSION.....	35
REFERENCES	37
BIOGRAPHICAL SKETCH	41

LIST OF TABLES

	Page
Table 1: Co-axial extrusion printer operating condition.....	13
Table 2: Parameters and level of the Factorial design	14
Table 3: Measurements of the printed tubular construct at different combinations of bioink.....	18
Table 4: Analysis of Variance of the Total width.....	19
Table 5: Analysis of Variance of the channel width.....	19
Table 6: Analysis of Variance of the wall thickness.....	20
Table 7: Model Summary	20
Table 8: Solutions from response surface optimizer.....	23
Table 9: Measurements of the printed tubular construct at a different flowrate.....	24
Table 10: Analysis of Variance of channel diameter.....	26
Table 11: Analysis of Variance of Total diameter.....	26
Table 12: Analysis of Variance of Wall thickness.....	27
Table 13: Model Summary	31
Table 14: Solutions from response surface optimizer.....	32

LIST OF FIGURES

	Page
Figure 1: Schematic view of the anatomy of an arterial wall	2
Figure 2: Classification of Bioprinting Technologies.....	4
Figure 3: Classification of hydrogels depending on crosslinking mechanisms	5
Figure 4: Co-axial Extrusion Printer set up in the biomanufacturing lab at UTRGV	10
Figure 5: Co-axial extrusion printing of hollow tubular structure (without cell) in the biomanufacturing lab at the Biomedical research building, UTRGV.....	11
Figure 6: Printed filament with different flowrate	12
Figure 7: Curvy channel on the printed tubular structure	13
Figure 8: Printed tubular structures at different flow rates and bioink concentrations.....	15
Figure 9: Confluent human aortic smooth muscle cell	16
Figure 10: Non-tubule filament with cell laden bioink, (left) green tag shows the live cells on the printed filament, and (right) red tag shows the dead cells on the printed filament. Images were taken by the fluorescence confocal microscope.....	17
Figure 11: Pareto charts of the standardized effects of alginate and CaCl ₂ concentration	21
Figure 12: Main Effects and interaction plots of alginate and CaCl ₂ concentration	22
Figure 13: Overlaid contour plot for alginate and CaCl ₂ concentration	23
Figure 14: Printed Tubular Structure after printing (a,c), and after injecting blue dye via channel(b,d, when)flow rate 600 µl/min(a,b) and flow rate 800 µl/min(c,d)	25

Figure 15: Normal plot (a, c, and e) and Pareto chart (b, d, and f) of the standardized effect of alginate concentration and flow rate	28
Figure 16: Normal Probability plot of the standardized residual.....	29
Figure 17: Main effects (a, c, and e) and Interaction plots (b, d, and f) of alginate concentration and flow rate	30
Figure 18: Overlaid contour plot of total width, channel width, and wall thickness	31
Figure 19: (a) Top surface view of the printed tubule in horizontal position, (b) Live cells on the printed tubule just after printing when the confocal microscope was focused on the mid surface level, and (c, d ,e, and f) live/dead assay on two different part of the same structure after 5 days of incubation.....	33
Figure 20: Cross sectional view of the printed structure and living cells after 5 days of incubation.....	34

CHAPTER I

INTRODUCTION

Tissue Engineering is a rapidly evolving discipline that combines the engineering and life sciences principles to fabricate an *in vitro* pharmacokinetic model to accurately predict human response to drug effects and potential toxic risk (Gu et al., 2020; Langer & Vacanti, 1999). Recently, three-dimensional (3D) printing is the most familiar technique in Tissue Engineering. It has become the most promising technique to fabricate living 3D cell-laden structures *in vitro* (Gu et al., 2020). Extrusion-based bioprinting is one of the 3D printing techniques widely used in TE to regenerate human organs and tissues.

One of the major steps of the bioprinting process is selecting the appropriate configuration of printing parameters as per the required pattern geometries. In the next step, materials including cells, growth factors, and hydrogels should be chosen carefully according to the requirement of the printed structures. For successful bioprinting, printability is important because the difference between a printed scaffold and the ideal design can impact the mechanical and biological properties, such as mechanical strength and cell functions (Naghieh & Chen, 2021). Printability is the ability to print a reproducible structure using the bioprinting technique. Flow behavior and physical properties of bioink, scaffold design, and printing processes such as crosslinking mechanism and printing parameters mainly affect printability (Naghieh et al., 2020). To construct the relationships between printability and printing Parameters is difficult because of

the presence of too many independent and inter-correlated factors. For this reason, it is necessary to identify and limit the number of significantly influential factors.

Bioengineering artificial vessels is the major interest area in 3D printing to replace the damage vessels as surgical options are limited(Xu et al., 2020).Blood vessel has three layers: tunica intima, tunica media, and tunica adventitia. In the tunica media zone, which is the medium part of the blood vessel, vascular smooth muscle cells are located. Figure 1 shows the blood vessel layers. Vascular smooth muscle cells (VSMC) are an important component of blood vessels because of its physiological functionality such as vasoconstriction and vasodilation. In addition, VSMC is associated with various diseases such as atherosclerosis and hypertension (Bacakova et al., 2018), Urinary bladder cancer, reproductive disorders, age-related focal loss of contractile vascular smooth muscle cells in retinal arterioles(Reagan et al., 2018), etc. Therefore, analysis of the behavior and orientation smooth muscle cells after printing is required to better understand the 3D bioprinting process of the blood vessel.

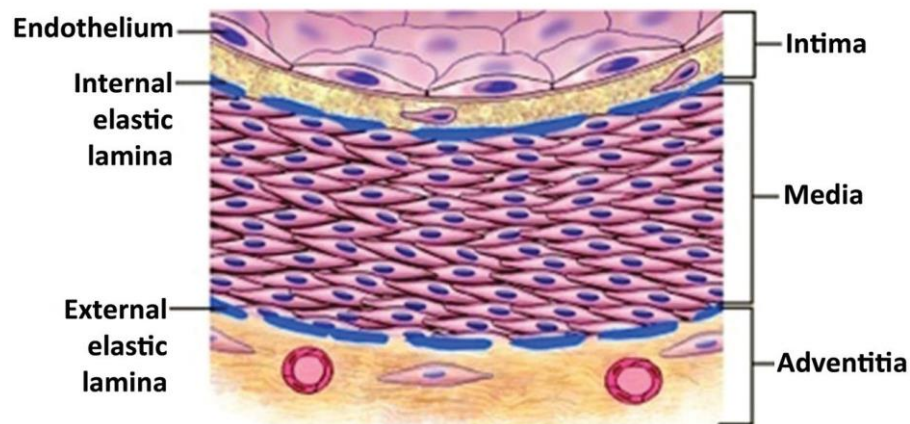


Figure 1: Schematic view of the anatomy of an arterial wall

In this study, a co-axial extrusion printer was used to fabricate a hollow tubular structure with human aortic smooth muscle cells. Printing a structure with cylindrical shape is difficult because of surface tension and gravity. For example, spreading can occur for high wettable

bioink material which leads to deterioration from the ideal design. To reduce the spreading of the printed strand, the printing substrate can be coated with hydrophobic material for a rougher surface (Vafaei et al., 2016). Otherwise, crosslinking time should be faster (Naghieh et al., 2018). Another study recommended high viscous bioink to reduce spreading (Udofia & Zhou, 2019). That means to fabricate tubular structure with proper dimension, crosslinking time, and the concentration of bioink are the major important factors. In this study, initial prints involved printing with bioink without cell to observe the process compatibility and printability. The design of experiment was used to identify the most significant influential factors and the response optimizer was used to find the optimum process parameter: bioink concentration, crosslinker concentration, and extrusion rate. In the next phase, a tubular structure with cell-laden bioink was fabricated to observe the cell orientation, cell distribution, and viability of the smooth muscle cells. Though some research works did printability analysis and statistical analysis of the extrusion based bioprinting technique (Gao et al., 2015; Naghieh & Chen, 2021), they did not provide any mathematical model. In addition, though one study investigated the printability of tubular structure by the micro-extrusion-based bioprinting process (Ding & Chang, 2018), process parameter optimization works for extrusion printing are very limited. So, this research can significantly contribute to improve the printability of extrusion based bioprinting system and help to reproduce the 3D structure with same pattern design. Ultimately, this study will contribute to the drug research and regenerative medicine.

CHAPTER II

LITERATURE REVIEW

3D bioprinting is a process to fabricate living structures with cell-laden bioinks. There are various types of 3D bioprinting techniques: droplet-based, extrusion-based, and photo-curing-based. Figure 2 shows the classification of bioprinting techniques(Gu et al., 2019).

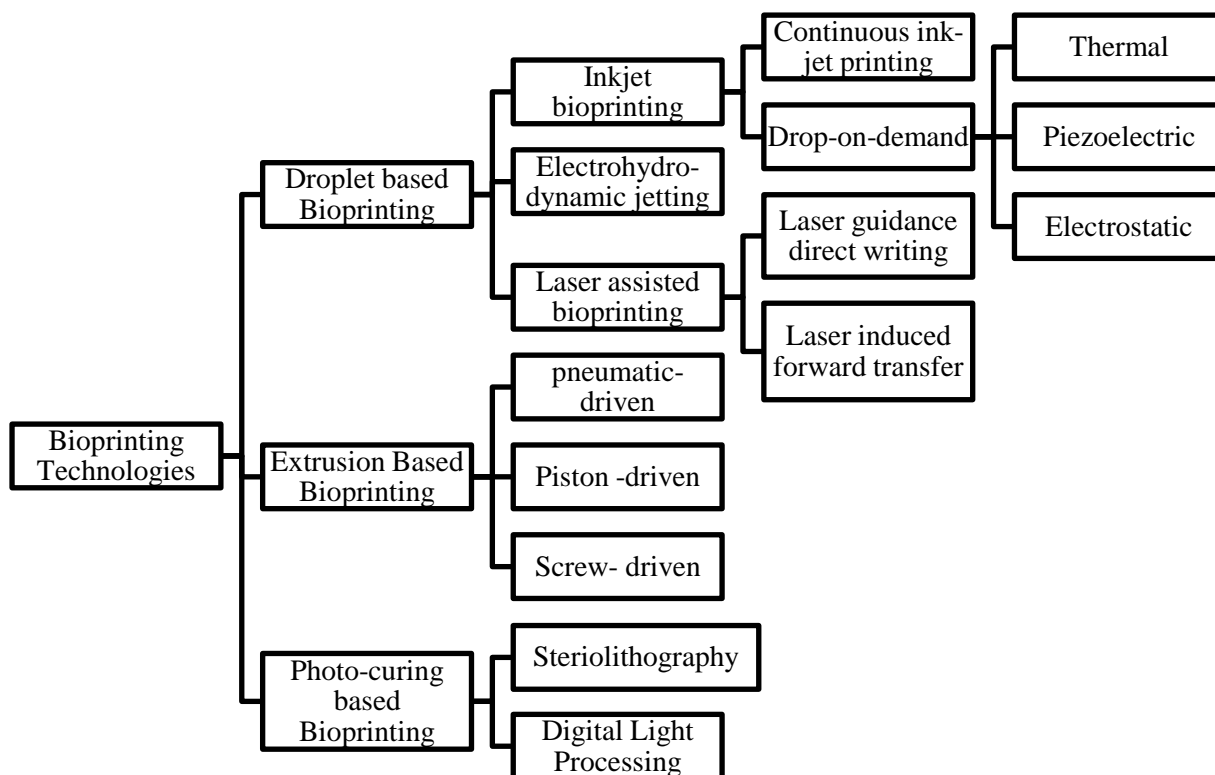


Figure 2: Classification of Bioprinting Technologies

Extrusion-based bioprinter is a medium resolution technique and it can deposit large volume of cells(Guillotin & Guillemot, 2011). In this process, a mixture of biomaterials and cells (bioink) is extruded, to form a 3D scaffold (Naghieh, 2020). Bioink needs to be crosslinked during or after printing to convert the liquid ink into hydrogels. Hydrogel consists of a group of polymeric materials, the hydrophilic structure which is capable of holding large amounts of water in their three-dimensional networks (Gulrez). Depending on the crosslinking mechanisms, hydrogels are classified into three categories(Ozbolat & Hospodiuk, 2016). Figure 3 shows the classification. Chemically crosslinked hydrogels are permanent and irreversible due to the chemical reaction and rearrangement of the atoms in a molecule . On the contrary, Physically crosslinked hydrogels are reversible due to the conformational changes(Panchal et al.; Ullah et al., 2015).

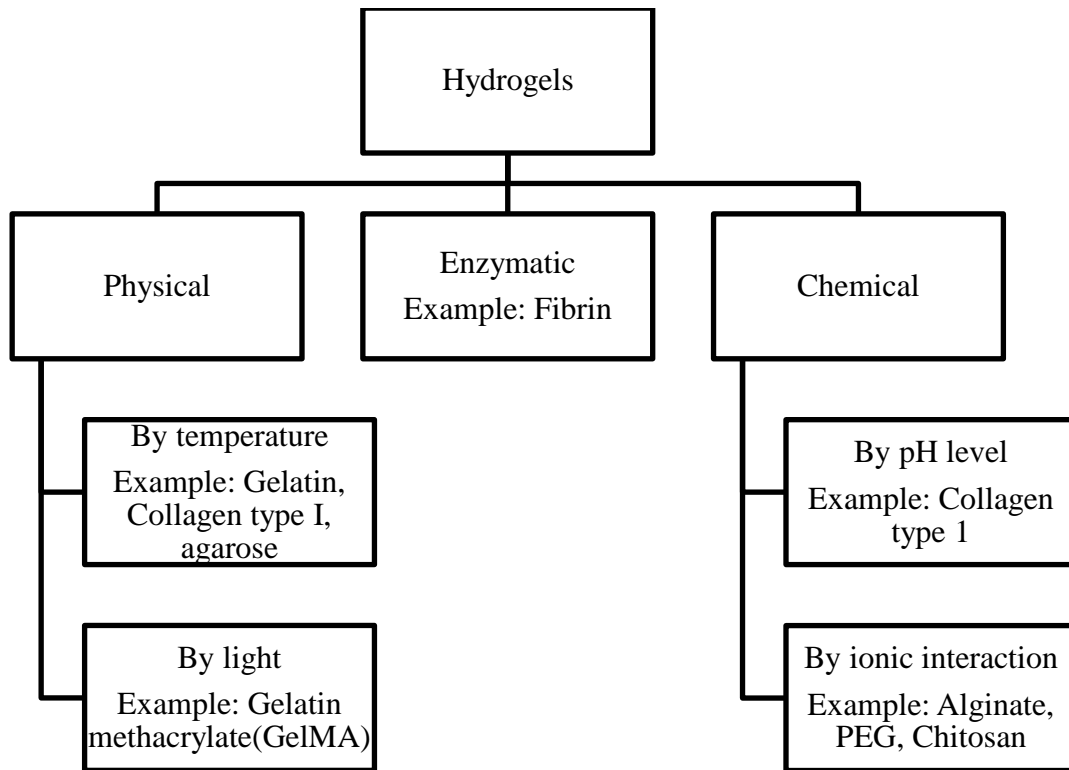
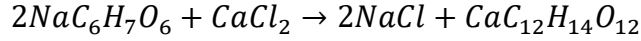


Figure 3: Classification of hydrogels depending on crosslinking mechanisms

One of the popular crosslinking mechanisms is the ionic interaction between alginate and Calcium Chloride solution. Sodium alginate ($NaC_6H_7O_6$) reacts with calcium chloride ($CaCl_2$) to make calcium alginate ($CaC_{12}H_{14}O_{12}$) which is a gelatinous substance.



This technique is widely used in extrusion printing to make hydrogels (Duan et al., 2013; Habib et al., 2018; Liu et al., 2018; Naghieh, 2020; Yang et al., 2018). One study used this crosslinking mechanism to print filament with microchannels by the coaxial extrusion printing process. In that study, two syringe pumps were used to dispense bioink and crosslinker calcium chloride solution through outer and inner nozzle respectively (Gao et al., 2015). When the two solution flows contacted each other, $CaCl_2$ diffused into the sodium alginate solution, and then crosslinking start. Thus, liquid bioink converted into calcium alginate ($CaC_{12}H_{14}O_{12}$) hydrogel which was the outer wall of the filament. Finally, a tubular structure with microchannel was formed. This study showed that crosslinking time decreases significantly when calcium chloride solutions were at high concentrations (Gao et al., 2015). In addition, the larger volume of Ca^{2+} ions lead to better mechanical stability immediately after printing (Naghieh et al., 2018). However, the higher stiffness reduces the permeability of alginate which leads to the decrease of cell viability and proliferation (Banerjee et al., 2009). For cell viability, a lower concentration of crosslinker is recommended and for faster crosslinking, a higher concentration of $CaCl_2$ is required. To overcome this dilemma, it is necessary to find the optimum $CaCl_2$ concentration for better printability. In addition, the flow rate is another important factor to improve printability. As crosslinking starts after two solutions flow contact each other, contact time is the crucial factor for printability. If the flow rate increase, the contact time will decrease, and if the flow rate decrease, the contact time will increase. So, for faster crosslinking, a higher flow rate is required.

However, the excessive flow rate can affect the scaffold dimension. For this reason, identifying the optimum flow rate is mandatory.

Alginate is a low-cost natural biopolymer that is obtained from seaweeds (Tønnesen & Karlsen, 2002). For cell encapsulation, alginate is one of the most utilized materials as bioink. However, some applications reported alginate shows poor cell proliferation and differentiation (Axpe & Oyen, 2016). As, alginate pore size range between 5 and 200 nm (Gombotz & Wee, 1998), it might be a reason for poor cell proliferation. Collagen can be incorporated in alginate to support cell growth and facilitate cell adhesion and cell differentiation (Xiao et al., 2017). Some studies reported that pure collagen has poor mechanical properties (Hospodiuk et al., 2017; Włodarczyk-Biegun & Del Campo, 2017). To overcome this limitation and improve printability, researchers used supportive hydrogels (Osidak et al., 2020). In one study, Collagen-alginate hydrogels were used in cartilage 3D bioprinting. This study reported, compared with alginate, the composite of alginate/collagen provides better mechanical strength (Yang et al., 2018).

Blood vessel system or vascularization is the key challenge in Tissue Engineering. Two main strategies are cell-based and scaffold-based (Novosel et al., 2011). Replacement or repair of a damaged small-diameter blood vessel with synthetic grafts is difficult. Therefore, bioprinting of artificial blood vessels of small diameter is a major area of interest. One study fabricated a 4 mm diameter bilayer blood vessel-like construct with gelatin methacryloyl (GelMA) bioink using a 3D micro-extrusion bioprinter (Xu et al., 2020). A co-axial extrusion printer can produce a hollow filament with a diameter in the micrometer range (Gao et al., 2015). This concept can be used to fabricate small blood vessels. Though this study did a statistical analysis to show the effect of process parameters on the printed tubular structure, they did not provide any mathematical model or did not investigate the optimum process parameter. However, an

optimum process parameter is necessary to ensure good printability and dimensional accuracy. For these reasons, the goal of this study is to identify the most significant factors with optimum values for co-axial extrusion printer.

In this study, a co-axial extrusion printer was used to fabricate a hollow tubular structure with the alginate hydrogels to investigate the printability and optimum process parameters. The objective was to ensure repeatable printing with the same dimension and consistency with these optimum process parameters. Finally, with these optimum parameters, the smooth muscle cell-laden tubular structure was printed to observe the cell viability and cell orientation in the tubular structure. This study result will help in the future research of fabricating a reproducible blood vessel-like construct by the co-axial extrusion printing process.

CHAPTER III

METHODOLOGY

3.1 Bioink Preparation

In this study, bioinks were prepared by mixing the sodium alginate with Collagen I (5 mg/ml). Sodium alginate (Na-Alg) solution was prepared by dissolving alginic acid, sodium salt (Sigma-Aldrich, Shanghai, China) into Phosphate-buffered Saline and placed in a magnetic stirrer for 24 h at room temperature to make the final Na-Alg solution with a concentration of 2%, 3%, and 4% (w/v). Similarly, calcium chloride (CaCl_2) solution was prepared as a crosslinker by dissolving CaCl_2 dihydrate (Sigma-Aldrich, Shanghai, China) into molecule water to make the final CaCl_2 solution with a concentration of 1-8% (w/v).

During mixing, all materials were kept inside the biosafety cabinet on ice to avoid early collagen gelation. Mixing was performed with a pipette (Dickman et al., 2020). Bioinks were prepared in two ways: without cell and with cell. At first, 3 different concentrations of bioinks were prepared (without cells) for the design of experiment. This experiment was conducted to find the optimum bioink concentration for better printing resolution. Then final bioink was prepared by mixing smooth muscle cells with the optimum concentration of bioink. Immediately prior to printing, cells were detached from cell culture flasks using 0.25% trypsin with 0.1% EDTA solution and centrifuged at 300 g for 5 minutes (Dickman et al., 2020). After

centrifugation, the supernatant was removed, and cells were resuspended in bioink on the ice at a density of 1 million cells per mL (HASMC).

3.2 Co-axial Extrusion Printing

In this study, a co-axial extrusion printing system is used to print the 3D tubular structure with human aortic smooth muscle cells. This system includes four subsystems: a co-axial nozzle with holder, 2 syringe pumps, a computer-controlled three-axis movable stage, and a computer that was used to control the motion stages and the syringe pump. Figure 4 shows the Co-axial printer setup in the Biomanufacturing lab at the Biomedical Research Building, UTRGV. The coaxial nozzle of 14,18 gauge was used in this study which had an outer needle with an inside diameter (I.D.) of 1.6 mm and an inner needle with an inside diameter (O.D.) of 0.838 mm. Two syringe pumps were used to dispense cell-laden bioink and crosslinker calcium chloride solution with individual flow rates through outer and inner nozzle respectively. Figure 5 shows the co-axial extrusion printing of the hollow tubular structure with the blue CaCl_2 flow through the inner nozzle.

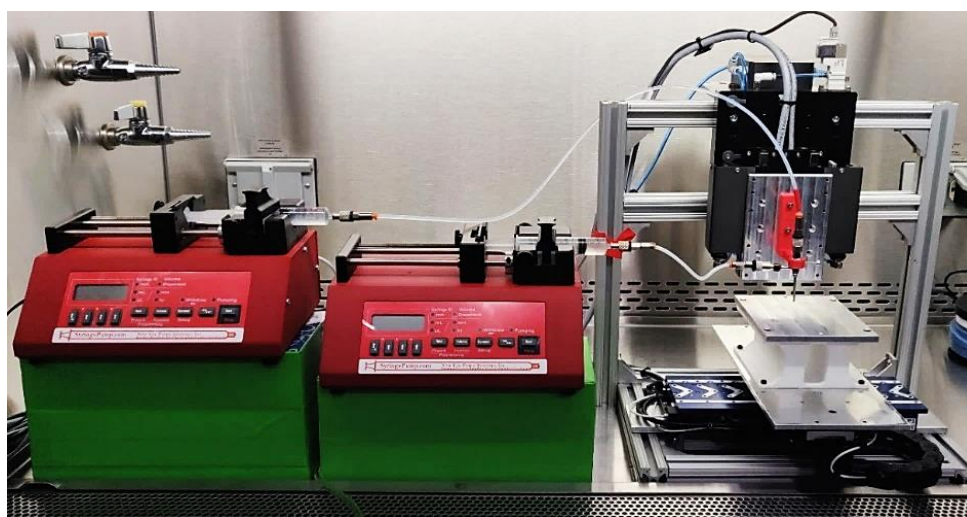


Figure 4: Co-axial Extrusion Printer set up in the biomanufacturing lab at UTRGV

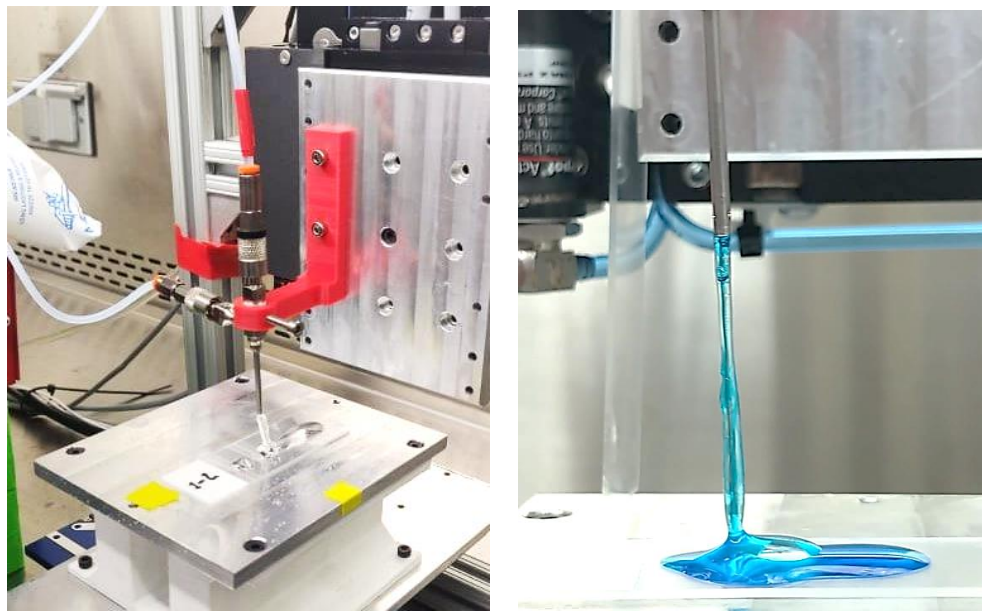


Figure 5: Co-axial extrusion printing of hollow tubular structure (without cell) in the biomanufacturing lab at the Biomedical research building, UTRGV

Flow rates of the CaCl_2 solution and the alginate bioink should match each other within a certain range to ensure continuous production and prevent nozzle clogging (Gao et al., 2015). For this reason, in this study, for bioink and crosslinker, similar flow rates were used to conduct the experiments. We found when the flow rates were 200 $\mu\text{l}/\text{min}$, the nozzle was clogged too fast and till 400 $\mu\text{l}/\text{min}$ there was discontinuous production. Beyond 800 $\mu\text{l}/\text{min}$ flow rates, materials overflow and the printed structures were not uniform. Figure 6 shows two printed filaments at a different flow rate. One filament has a uniform width, and another is not uniform. For these reasons, for successful bioprinting, find out the optimum flow rate is necessary.

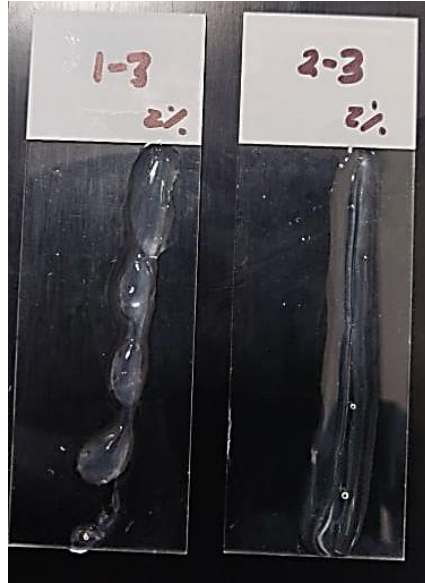


Figure 6: Printed filament with different flowrate

In addition, for successful bioprinting, the extrusion rate of the filament and the stage movement speed should also match each other. A higher extrusion rate than the stage movement speed is responsible for curvy channels. On the other hand, a lower extrusion rate than the stage movement speed is the reason not only for the dragging of the deposited filaments but also for the stretched filament (Gao et al., 2015; Liu et al., 2018). When the stage speed is higher, the extruded filament become thinner due to the tension generation along the deposition direction. It may also break down the extruded filament results in a discontinuous material deposition (Habib et al., 2018). Figure 7 shows the curvy channel when the extrusion rate was higher than the stage movement speed.



Figure 7: Curvy channel on the printed tubular structure

In this study, filament extrusion speed, $v = 4q/\pi d^2$, where q is the flow rate of the filament, d is the filament diameter (Gao et al., 2015). When the printing was performed with 1% sodium alginate solution with a dispensing rate of 1000 $\mu\text{l}/\text{min}$ and 2% calcium chloride solution was dispensed at 1000 $\mu\text{l}/\text{min}$. The flow rate of the filament q was approximate at 1000 $\mu\text{l}/\text{min}$ and the filament diameter was 1600 μm , so the filament extrusion speed was 8.34 mm/sec. The co-axial extrusion printing experiment was carried out under the fixed conditions mentioned in Table 1.

Table 1: Co-axial extrusion printer operating condition

Parameters	Values	Units
Nozzle diameter (inside diameter)	Inner nozzle diameter = 0.838, Outer nozzle diameter=1.6	mm
Nozzle distance from the substrate	500	μm
Stage Movement Speed	500	mm/min
Room Temperature	25	$^{\circ}\text{C}$

3.3 Experiment Design

. The goal of this experiment was to find the optimum process parameter which will result in less difference of the printed tubular structure's dimension concerning the original nozzle diameter. In this study, response surface methodology was conducted with three input parameters: concentration of alginate solution, the concentration of calcium chloride solution, and flow rate of these two solutions to evaluate the printability of a hollow tubular structure. The output parameters: tube diameter, channel diameter, and wall thickness of the hollow tube. The experimental data were used to finalize the parameter ranges. The selected input factors with their levels are shown in Table 2.

Table 2: Parameters and level of the Factorial design

Symbol	Parameter	Level			Unit
		1	2	3	
CaCl ₂ %	Concentration of CaCl ₂	1	2	3	Multiplying factor with NaAlg %
Alg %	Concentration of NaAlg	1	1.5	2	%
Flow rate	Similar flow rate for bioink and CaCl₂	400	600	800	μl/min

2

Figure 8 shows the Printed tubular structures at different flow rates and bioink concentrations. The printed structure is observed under the optical microscope. The image was captured by the camera through the eyepiece of the microscope. ImageJ software was used to measure the dimension of the total diameter and channel diameter. The dark area was the gelled wall of the tubular structure which is formed due to the crosslinking mechanism between alginate and Calcium Chloride

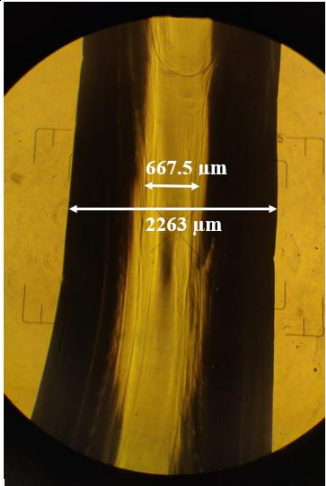
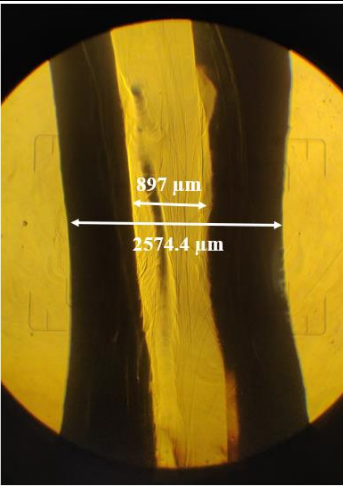
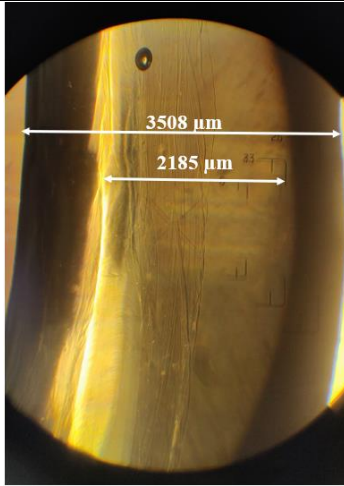
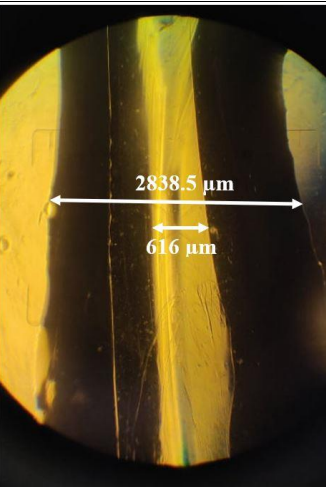
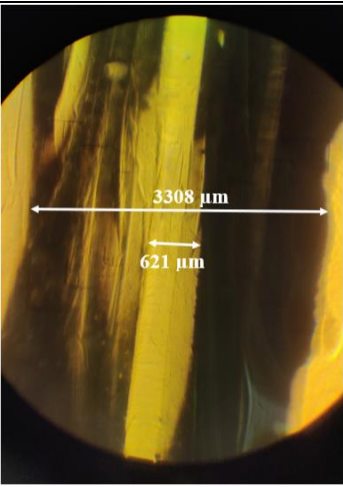
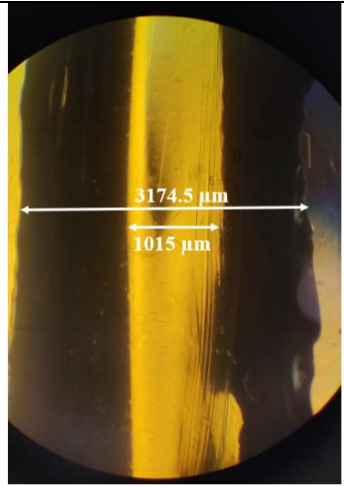
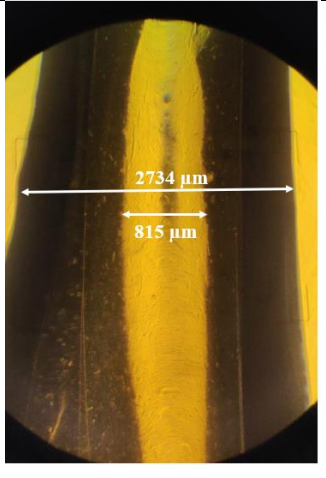
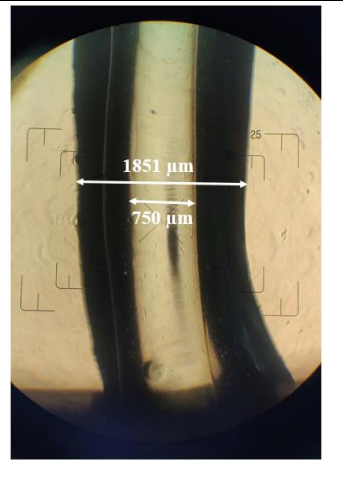
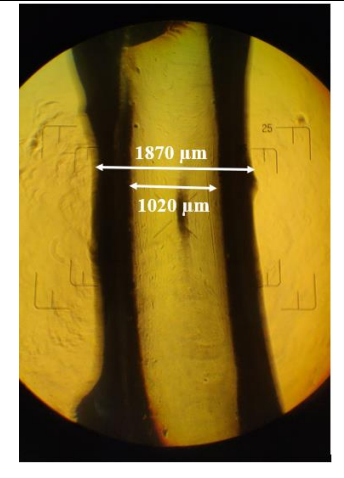
Alginate %	Flow Rate 400 $\mu\text{l}/\text{min}$	600 $\mu\text{l}/\text{min}$	800 $\mu\text{l}/\text{min}$
1			
1.5			
2			

Figure 8: Printed tubular structures at different flow rates and bioink concentrations

Figure 8 shows that for 1% alginate, when flow rate was increased from 400 to 800 $\mu\text{l}/\text{min}$, the channel diameter also increased from 667.5 to 2185 μm . However, flow rate didn't have any significant effect on the total diameter dimension. Figure 8 also shows that for 800 $\mu\text{l}/\text{min}$ flow rate, when alginate concentration increased from 1% to 2%, total diameter was reduced from 3508 μm to 1870 μm . However, alginate concentration had not that much effect on channel diameter.

3.4 Cell Culturing

Human aortic smooth muscle cells (Cell Systems) were expanded (passage 4–6) and used in this study. SMCs were cultured in complete classic medium with serum and culture boostTM (4Z0-500, Cell Systems, USA) supplemented with 10% (v/v) fetal bovine serum (FBS) and 1% (v/v) antibiotic-antimycotic solution. Cell type was incubated at 37 °C, 5% CO₂, and 95% relative humidity. Figure 9 shows the confluent human aortic smooth muscle cells.

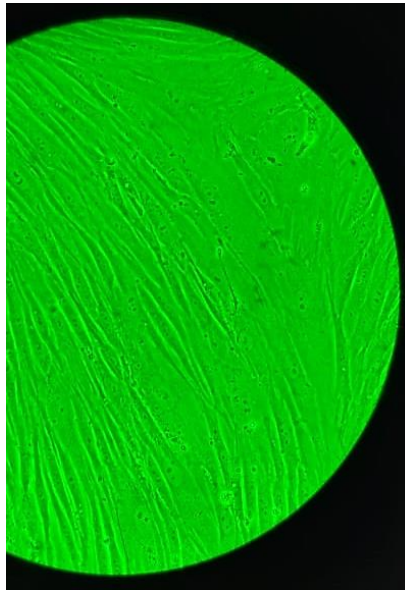


Figure 9: Confluent human aortic smooth muscle cell

3.5 Cell Viability in proposed bioink

The viability of Human Aortic Smooth Muscle Cells (HASMC) in the proposed bioink was observed using a LIVE/DEAD cell imaging kit (488/570, Invitrogen, USA) according to the manufacturer's instructions. Cell viability was checked after 5 days of printing. The printed structure was kept in a dark incubator, at 37 °C and 5% CO₂. After 5 days, just after staining, samples were kept at 70° F for 30 minutes. Fluorescence confocal microscopy (Nikon) was used to evaluate the live (green) and dead (red) staining cells in the printed constructs. Each sample was photographed and analyzed using Image J software, and the cell viability was then expressed as a percentage of the number of live cells to the number of total cells per area. Figure 10 shows the live/dead assay of the printed line just after printing. The combination of that bioink was 1.5 % alginate and 5mg/ml collagen I. 3% calcium chloride was used as crosslinker.

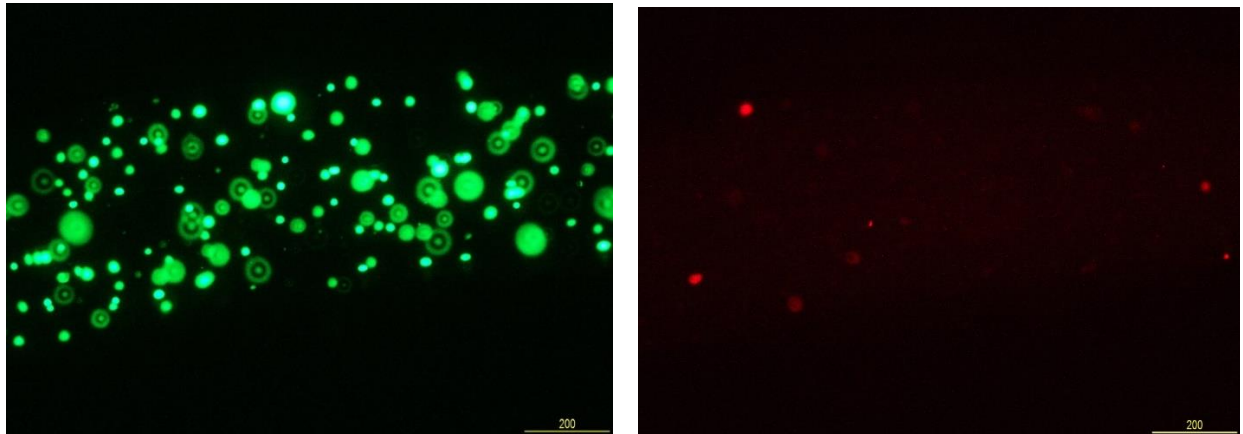


Figure 10: Non-tubule filament with cell laden bioink, (left) green tag shows the live cells on the printed filament, and (right) red tag shows the dead cells on the printed filament. Images were taken by the fluorescence confocal microscope.

CHAPTER IV

RESULT AND DISCUSSION

4.1 Printability assessment with the different concentrations of solutions

In this study, the composite of alginate and collagen solution was used as bioink. Collagen concentration was fixed at 2.5 mg/ml. The response surface methodology was conducted with two input parameters: concentration of alginate solution, and calcium chloride solution for the three responses: total diameter, channel diameter, and wall thickness of the hollow tube. Table 3 shows the average measurements of the printed structures which were printed with the 9 different bioink combinations.

Table 3: Measurements of the printed tubular construct at different combinations of bioink

Alginate solution	Calcium Chloride solution	Total Diameter of the construct	Wall thickness of the construct	Channel Diameter of the construct
%	multiply with alginate %	µm	µm	µm
1.0	1	1700.00	220.000	1262.00
1.0	2	2194.00	558.000	1039.00
1.0	4	1829.00	480.405	1018.86
1.5	1	999.78	194.555	662.47
1.5	2	1607.61	308.000	978.50
1.5	4	2332.66	540.080	1368.72
2.0	1	1855.72	677.860	500.00
2.0	2	1899.95	604.095	842.18
2.0	4	2135.79	676.305	870.00

The corresponding statistical results were obtained by Minitab® 19 software. In this analysis, a 90% confidence interval was considered, so the significance level $\alpha=0.1$. For the significance level, $\alpha=0.1$, if the p-value of the factor is less than 0.1, it will be a significant parameter.

ANOVA table for tubular structure's total width, channel width, and wall thickness are shown in Table 4, 5, and 6 respectively.

Table 4: Analysis of Variance of the Total width

Source	DF	Adj SS	Adj MS	F-Value	P-Value
Model	3	476062	158687	1.04	0.451
Linear	2	461367	230684	1.51	0.307
Alginate %	1	7325	7325	0.05	0.835
Calcium Chloride %	1	454043	454043	2.98	0.145
2-Way Interaction	1	17289	17289	0.11	0.750
Alginate %*Calcium Chloride %	1	17289	17289	0.11	0.750
Error	5	762993	152599		
Total	8	1239055			

Table 5: Analysis of Variance of the channel width

Source	DF	Adj SS	Adj MS	F-Value	P-Value
Model	3	389368	129789	3.25	0.119
Linear	2	280256	140128	3.50	0.112
Alginate %	1	169816	169816	4.25	0.094
Calcium Chloride %	1	110440	110440	2.76	0.157
2-Way Interaction	1	74436	74436	1.86	0.231
Alginate %*Calcium Chloride %	1	74436	74436	1.86	0.231
Error	5	199968	39994		
Total	8	589336			

Table 6: Analysis of Variance of the wall thickness

Source	DF	Adj SS	Adj MS	F-Value	P-Value
Model	3	146724	48908	1.82	0.260
Linear	2	128509	64254	2.39	0.187
Alginate %	1	73018	73018	2.72	0.160
Calcium Chloride %	1	55490	55490	2.07	0.210
2-Way Interaction	1	9601	9601	0.36	0.576
Alginate %*Calcium Chloride %	1	9601	9601	0.36	0.576
Error	5	134307	26861		
Total	8	281031			

Table 4 shows that all p values are greater than 0.1 which means alginate concentration and calcium chloride concentration have no significant effect on the total width of the tubular structure. Table 5 shows that the alginate concentration's P-value is 0.094, which means it is the only significant factor for the channel width of the hollow tubular structure. Finally, Table 6 shows that these two factors have no significant effect on the wall thickness of the tubular structure.

Table 7: Model Summary

	S	R-sq	R-sq(Yeong et al.)	R-sq(pred)
Total width	390.639	38.42%	1.47%	0.00%
Channel width	199.98	66.07%	45.71%	0.00%
Wall thickness	163.895	52.21%	23.53%	0.00%

Table 7 shows the model summary of the factorial design.

Figure 11 (a), (b), and (c) illustrates the standardized effects of the input parameters on the channel diameter, total diameter, and wall thickness respectively. These Pareto charts show that alginate concentration has a marginal effect on channel diameter, and it has no significant effect on total diameter and wall thickness. In addition, Figure 11 illustrates that calcium chloride concentration has no significant effect on the tubular structure dimension.

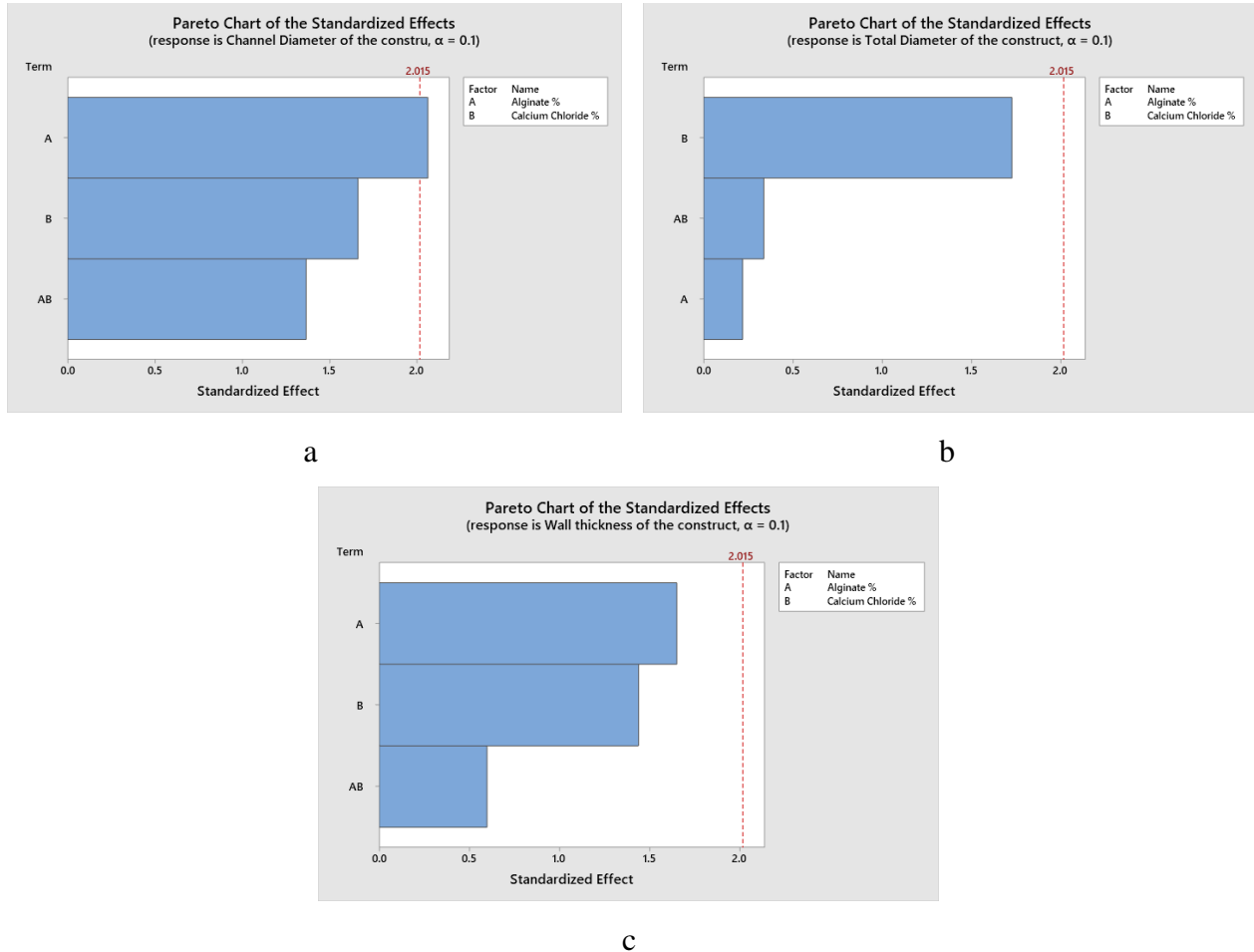


Figure 11: Pareto charts of the standardized effects of alginate and CaCl_2 concentration

Figure 12(a, c, and e) illustrate that when CaCl_2 concentration increased, channel diameter, total diameter, and wall thickness of the tubule increased. In addition, these main effects plots illustrate that when alginate concentration increased, channel diameter decreased. However, alginate concentration did not affect the tubule's total diameter and wall thickness in a

distinct trend. However, Figure 12(b, d, and f) show that for the tubule's dimension, there are no strong interactions between alginate and CaCl_2 concentration.

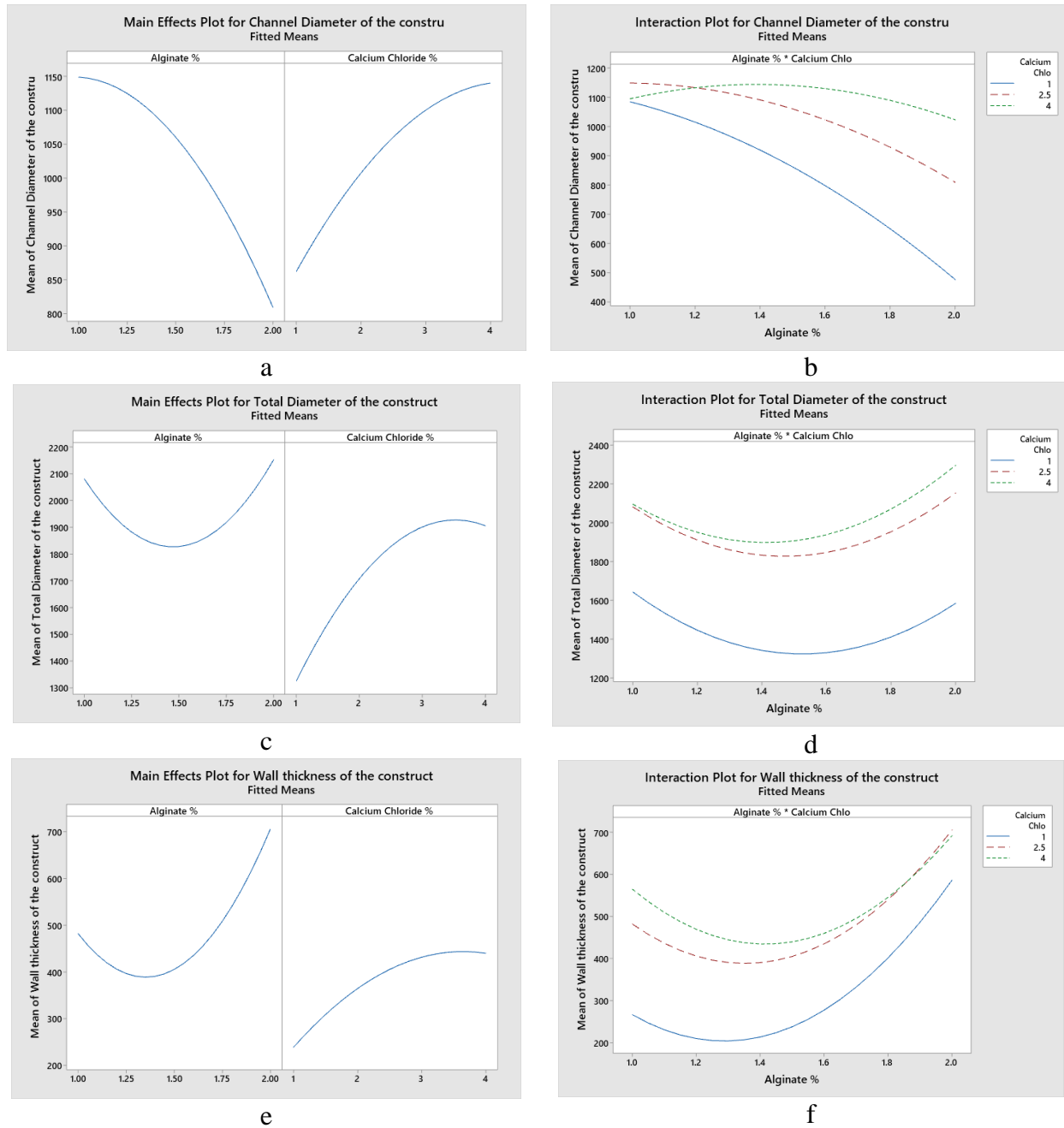


Figure 12: Main Effects and interaction plots of alginate and CaCl_2 concentration

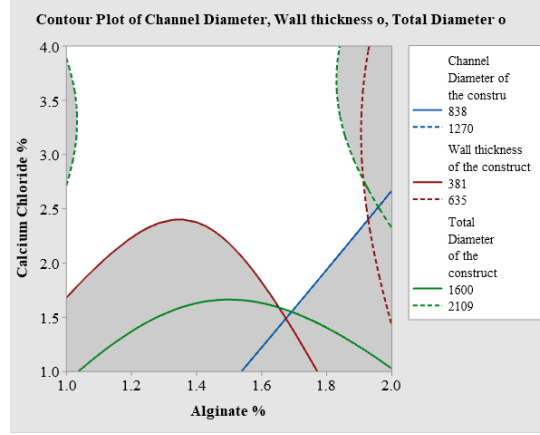


Figure 13: Overlaid contour plot for alginate and CaCl_2 concentration

Figure 13 shows the overlaid contour plot of channel diameter, total diameter, and wall thickness. As the objective is to find the optimum parameter to print a structure with a similar dimension of the nozzle, the range limit was set here as per the nozzle dimension. For example, the inner nozzle's inside diameter was $838 \mu\text{m}$ and the outside diameter was $1270 \mu\text{m}$. So, this is the selected range for the contour plot of the channel diameter. Similarly, the wall thickness range is $381\text{--}635 \mu\text{m}$, and the total diameter range is $1600\text{--}2109 \mu\text{m}$. For these ranges, the overlaid contour plot shows the white surface area which is the optimum parameter zone. Figure 13 illustrates that to get the best result, calcium chloride concentration should be greater than 1.5 multipliers with alginate concentration. Table 8 shows that for collagen-alginate bioink, 1.7% alginate, 1.5 times calcium chloride concentration are the optimum parameter to get the required dimension of the printed structure.

Table 8: Solutions from response surface optimizer

Solution	Alginate %	Calcium Chloride %	Channel Diameter Fit	Wall thickness Fit	Total Diameter Fit	Composite Desirability
		%				
1	1.69320	1.54944	838.000	397.810	1599.99	0.833687

4.2 Printability assessment with the process parameter

In this study, pure alginate bioink with three different concentrations was used to run the experiments and the concentrations of crosslinker were 2 times the bioink concentration. Then response surface methodology was conducted with two input parameters: concentration of alginate solution, and extrusion flow rate to optimize the printing process parameter to fabricate a hollow tubular structure with the almost similar dimensions of the nozzle. After printing with 9 experimental set up based on the general full factorial design, the obtained results are reported in Table 9.

Table 9: Measurements of the printed tubular construct at a different flowrate

Alginate	CaCl ₂	Flow rate	Left Wall	Right wall	Channel Thickness	Total diameter	Wall thickness
1%	2%	400	764	764	677.5	2263	764
1%		600	758	854	897	2574.4	806
1%		800	861	714	2185	3508	787.5
1.50%	3%	400	1045.8	1036.42	616	2838.56	1041.11
1.50%		600	1392	1400	621	3308	1396
1.50%		800	1147	1008	1015	3174.5	1077.5
2%	4%	400	972	944	815	2734	958
2%		600	588	570	750	1851	579
2%		800	490	410	1020	1870	450

Figure 14 shows the stable printed tubular structure with 2% alginate and 4% CaCl₂.

Figure 14 (a,c) shows the hollow tube when the flow rate was 600 and 800 $\mu\text{l}/\text{min}$ respectively.

Figure 14 (b,d) shows that blue dye passes through the hollow channel.

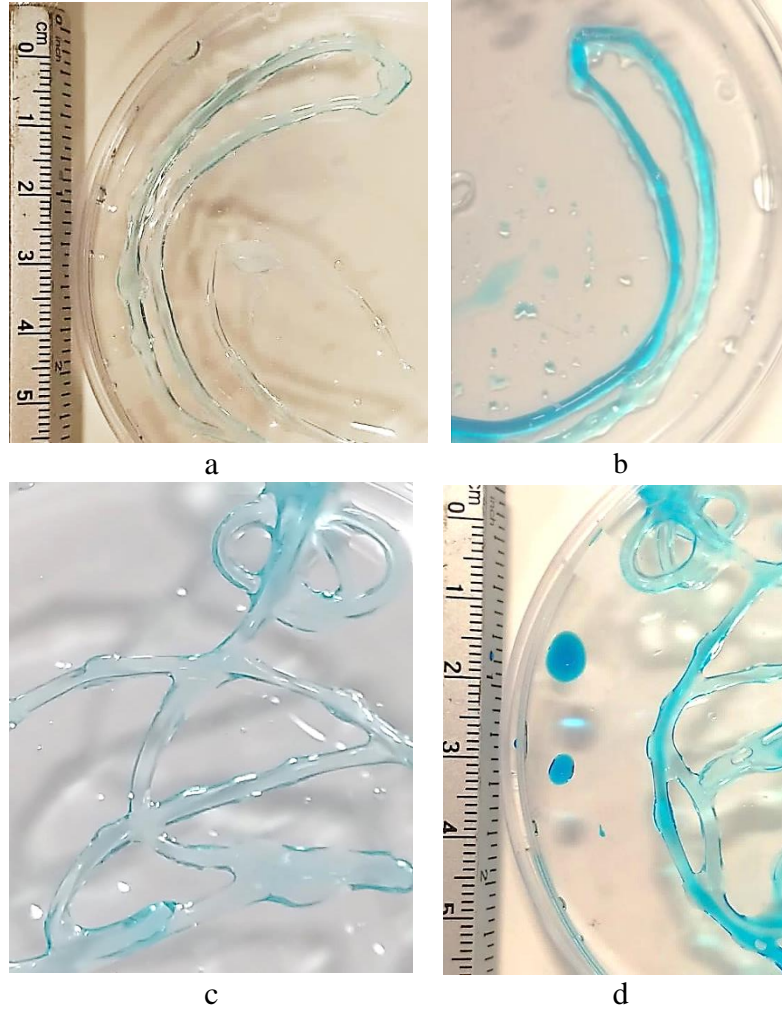


Figure 14: Printed Tubular Structure after printing (a,c), and after injecting blue dye via channel(b,d, when)flow rate 600 $\mu\text{l}/\text{min}$ (a,b) and flow rate 800 $\mu\text{l}/\text{min}$ (c,d)

The corresponding statistical results were obtained by Minitab[®] 19 software. In this analysis, a 90% confidence interval was considered, so the significance level $\alpha=0.1$. For the significance level, $\alpha=0.1$, if the p-value of the factor is less than 0.1, it will be a significant parameter. ANOVA table for tubular structure's total width, channel width, and wall thickness are shown in Table 10, 11, and 12 respectively.

Table 10: Analysis of Variance of channel diameter

Source	DF	Adj SS	Adj MS	F-Value	P-Value
Model	5	1763801	352760	8.44	0.055
Linear	2	972980	486490	11.64	0.039
Alginate	1	229908	229908	5.50	0.101
Flow rate	1	743072	743072	17.78	0.024
Square	2	366694	183347	4.39	0.129
Alginate*Alginate	1	188191	188191	4.50	0.124
Flow rate*Flow rate	1	178503	178503	4.27	0.131
2-Way Interaction	1	424127	424127	10.15	0.050
Alginate*Flow rate	1	424127	424127	10.15	0.050
Error	3	125396	41799		
Total	8	1889197			

Table 11: Analysis of Variance of Total diameter

Source	DF	Adj SS	Adj MS	F-Value	P-Value
Model	5	2660325	532065	7.24	0.067
Linear	2	681269	340635	4.63	0.121
Alginate	1	595602	595602	8.10	0.065
Flow rate	1	85667	85667	1.16	0.359
Square	2	867085	433543	5.90	0.091
Alginate*Alginate	1	819934	819934	11.15	0.044
Flow rate*Flow rate	1	47151	47151	0.64	0.482
2-Way Interaction	1	1111970	1111970	15.12	0.030
Alginate*Flow rate	1	1111970	1111970	15.12	0.030
Error	3	220612	73537		
Total	8	2880937			

Table 12: Analysis of Variance of Wall thickness

Source	DF	Adj SS	Adj MS	F-Value	P-Value
Model	5	540406	108081	3.26	0.180
Linear	2	56345	28173	0.85	0.510
Alginate	1	22878	22878	0.69	0.467
Flow rate	1	33467	33467	1.01	0.389
Square	2	413437	206719	6.23	0.085
Alginate*Alginate	1	400429	400429	12.08	0.040
Flow rate*Flow rate	1	13008	13008	0.39	0.576
2-Way Interaction	1	70623	70623	2.13	0.241
Alginate*Flow rate	1	70623	70623	2.13	0.241
Error	3	99474	33158		
Total	8	639880			

Table 10 shows that flow rate and alginate*flow rate interaction have P values smaller than 0.1 which means these two have a significant effect on the channel diameter of the tubular structure. Table 11 shows that alginate concentration's P-value is 0.065 and alginate* flow rate's P-value is 0.030, that means these are the significant factor for the total diameter of the hollow tubular structure. Finally, Table 12 shows that the concentration of alginate and flow rate has no significant effect on the wall thickness of the tubular structure.

Figure 15 illustrates the normal plot (left column) and Pareto charts (right column) of the standardized effects of the input parameters respectively. Figures 15 (a and b) show that flow rate is the most significant factor for the channel diameter. In addition, the interaction between alginate concentration and the flow rate has a significant effect on the channel diameter and the total diameter. Figure 15 (d) illustrates that alginate concentration has a limited effect on the total

diameter dimension. Finally, figure 15 (f) shows that these factors are not significant for the wall thickness of the printed structure.

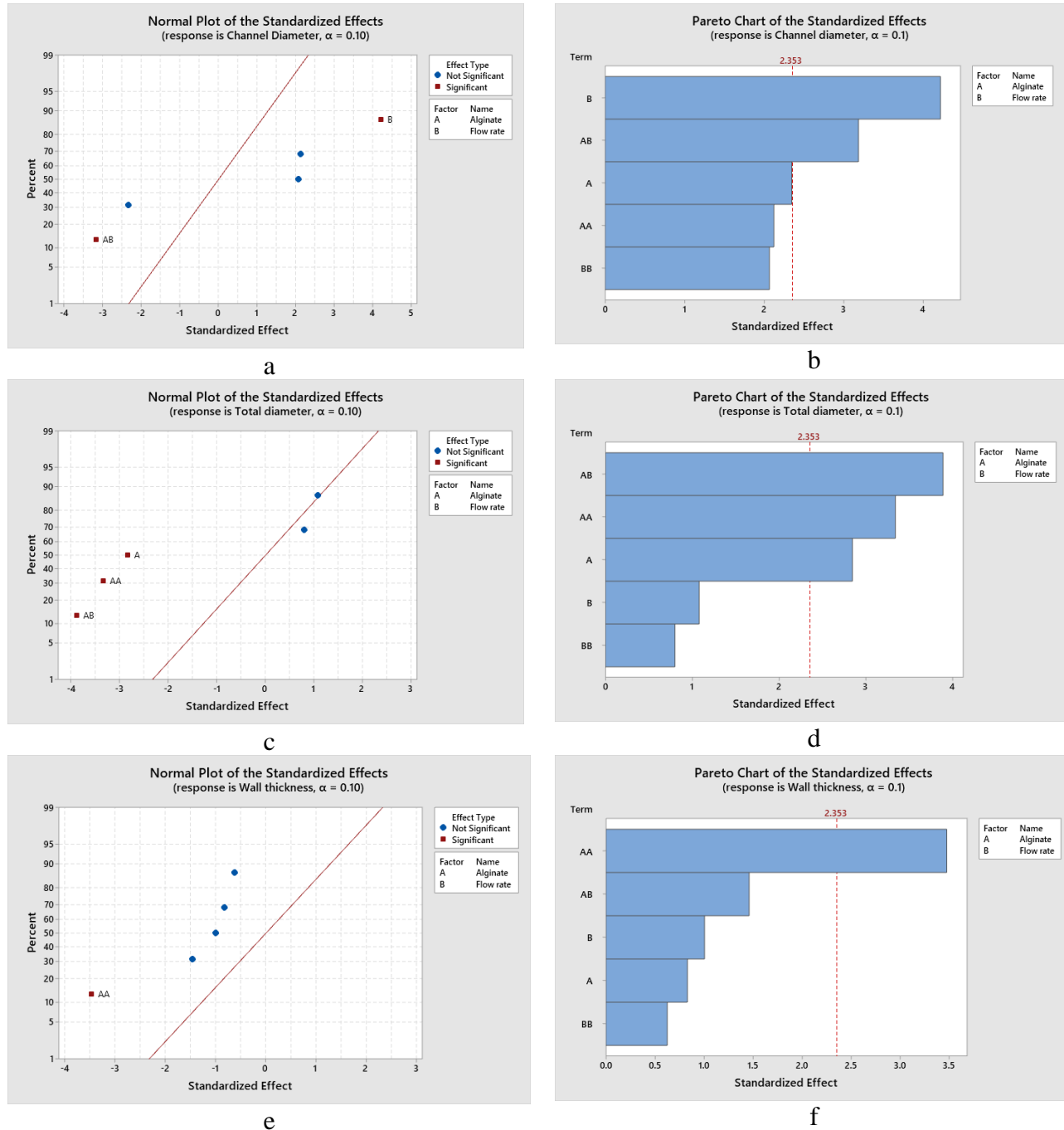
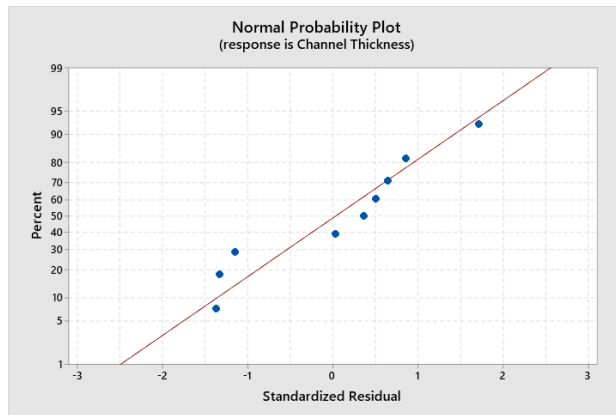
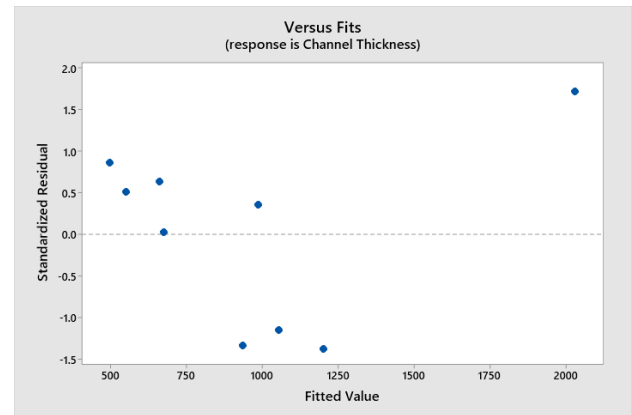


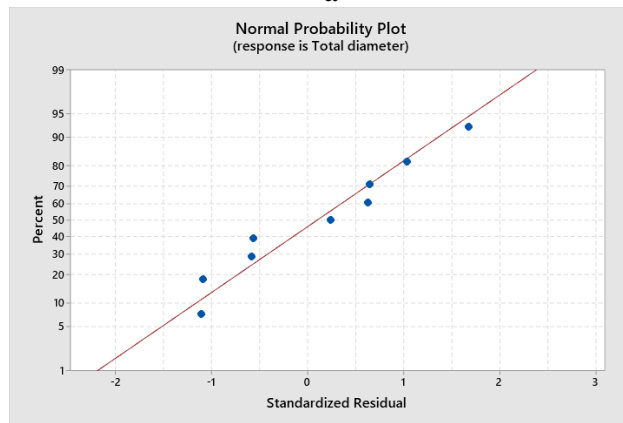
Figure 15: Normal plot (a, c, and e) and Pareto chart (b, d, and f) of the standardized effect of alginate concentration and flow rate



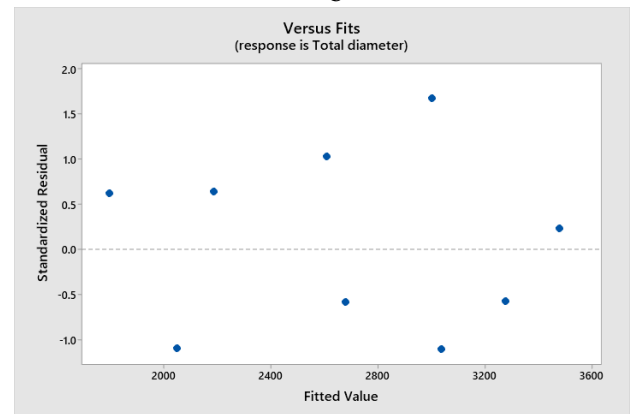
a



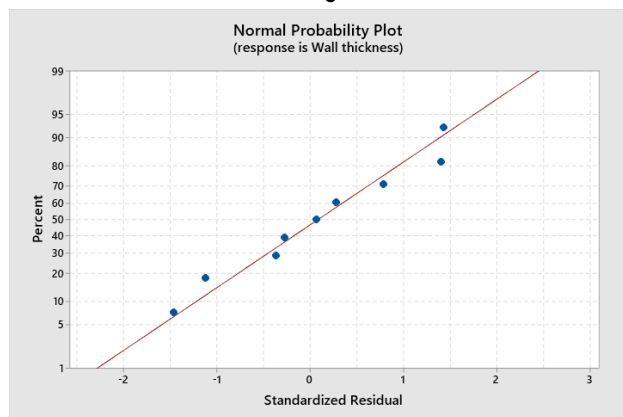
b



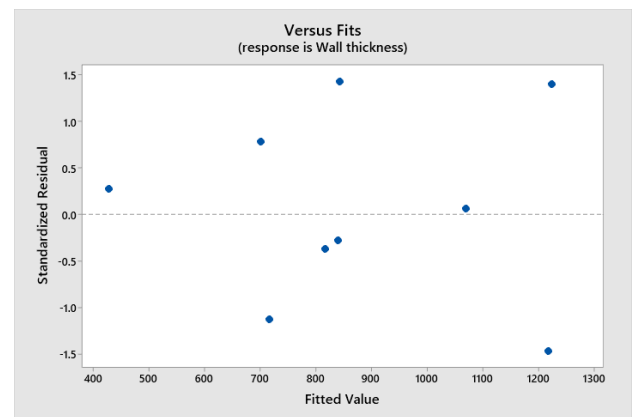
c



d



e



f

Figure 16: Normal Probability plot of the standardized residual

Figure 16 shows the normal probability plot of the standardized residual. It illustrates that all data points are within the acceptable range.

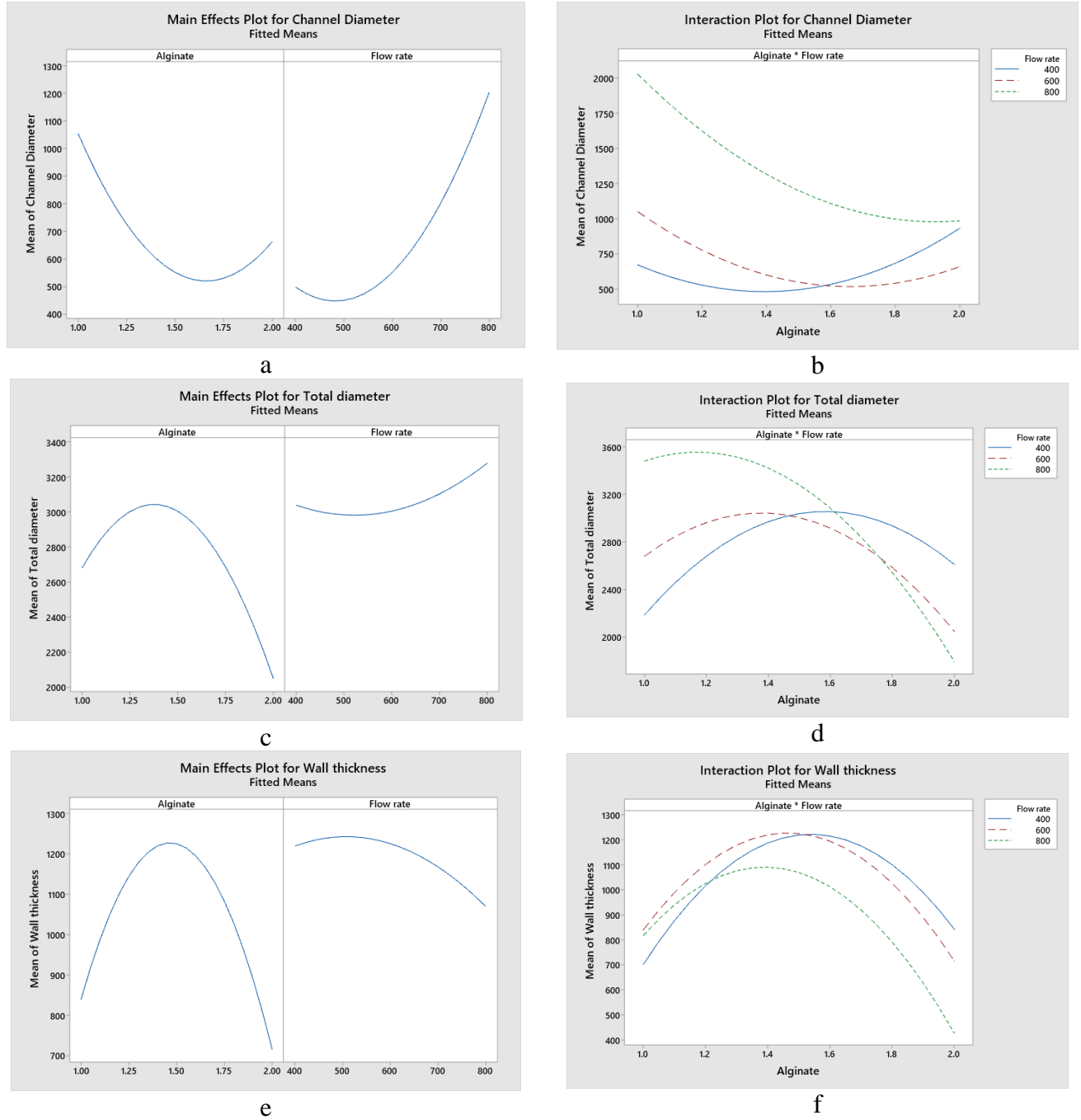


Figure 17: Main effects (a, c, and e) and Interaction plots (b, d, and f) of alginate concentration and flow rate

Figure 17 (a, c, and e) illustrate that when CaCl_2 or Na-Alg solution flow rate increased, channel diameter and a total diameter of the tubule increased, however, wall thickness

decreased. In addition, these main effects plots illustrate that alginate solution concentration did not affect the tubule diameter in a distinct trend. However, Figure 17 (b, d) shows that for total diameter, there is a strong interaction between alginate % and flow rate.

Table 13: Model Summary

	S	R-sq	R-sq(Yeong et al.)	R-sq(pred)
Total width	271.178	92.34%	79.58%	40.80%
Channel width	204.447	93.36%	82.30%	21.81%
Wall thickness	182.094	84.45%	58.54%	0.00%

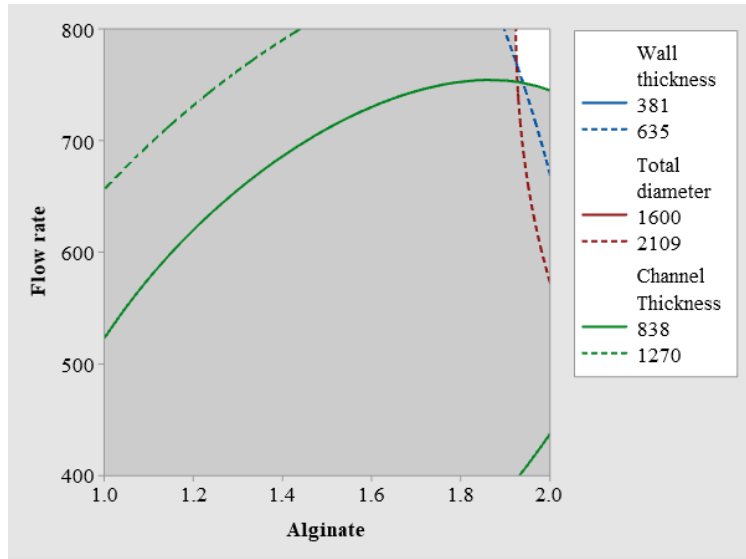


Figure 18: Overlaid contour plot of total width, channel width, and wall thickness

Figure 18 shows the overlaid contour plot of channel diameter, total diameter, and wall thickness. As the objective is to find the optimum parameter to print a structure with similar dimensions of the nozzle, the range limit was set here as per the nozzle dimension. For example, the inner nozzle's inside diameter was 838 μm and the outside diameter was 1270 μm . So, this is

the selected range for the contour plot of the channel diameter. Similarly, the wall thickness range is 381-635 μm , and the total diameter range is 1600-2109 μm . For these ranges, the overlaid contour plot shows the white surface area which is the optimum parameter zone. Figure 18 illustrates that to get the best result, alginate concentration should be greater than 1.9% and flow rate should be greater than 700 $\mu\text{l}/\text{min}$. Table 14 shows that for pure alginate bioink, 2% alginate, 780 $\mu\text{l}/\text{min}$ are the optimum parameter to get the required dimension of the printed structure.

Table 14: Solutions from response surface optimizer

Solution	Alginate	Flow rate	Wall thickness Fit	Total diameter Fit	Channel Thickness Fit	Composite Desirability
1	2	779.798	464.326	1806.82	927.581	0.935877

4.3 3D printing with cell-laden bioink

After finding the optimum process parameter, the cell-laden tubular structure was printed. Figure 19 (a) shows the microscopic view of the 3D printed tubular structure with human aortic smooth muscle cells. After 5 days, the live/dead assay was evaluated with fluorescence staining kits. The red color represents a dead cell and green represents live cells. Two parts of the same structure were stained and observed under the confocal microscope. Figure 19 (b) shows that cell density is comparatively lower in the middle zone as it is the channel area of the tubular structure. Figure 19 (e) shows that very few cells were elongated and the layer difference is clear. That illustrates it was a 3D structure. In addition, figure 19 illustrates that smooth muscle cells can survive in the alginate bioink though it has a very small pore size such as 500 nm.

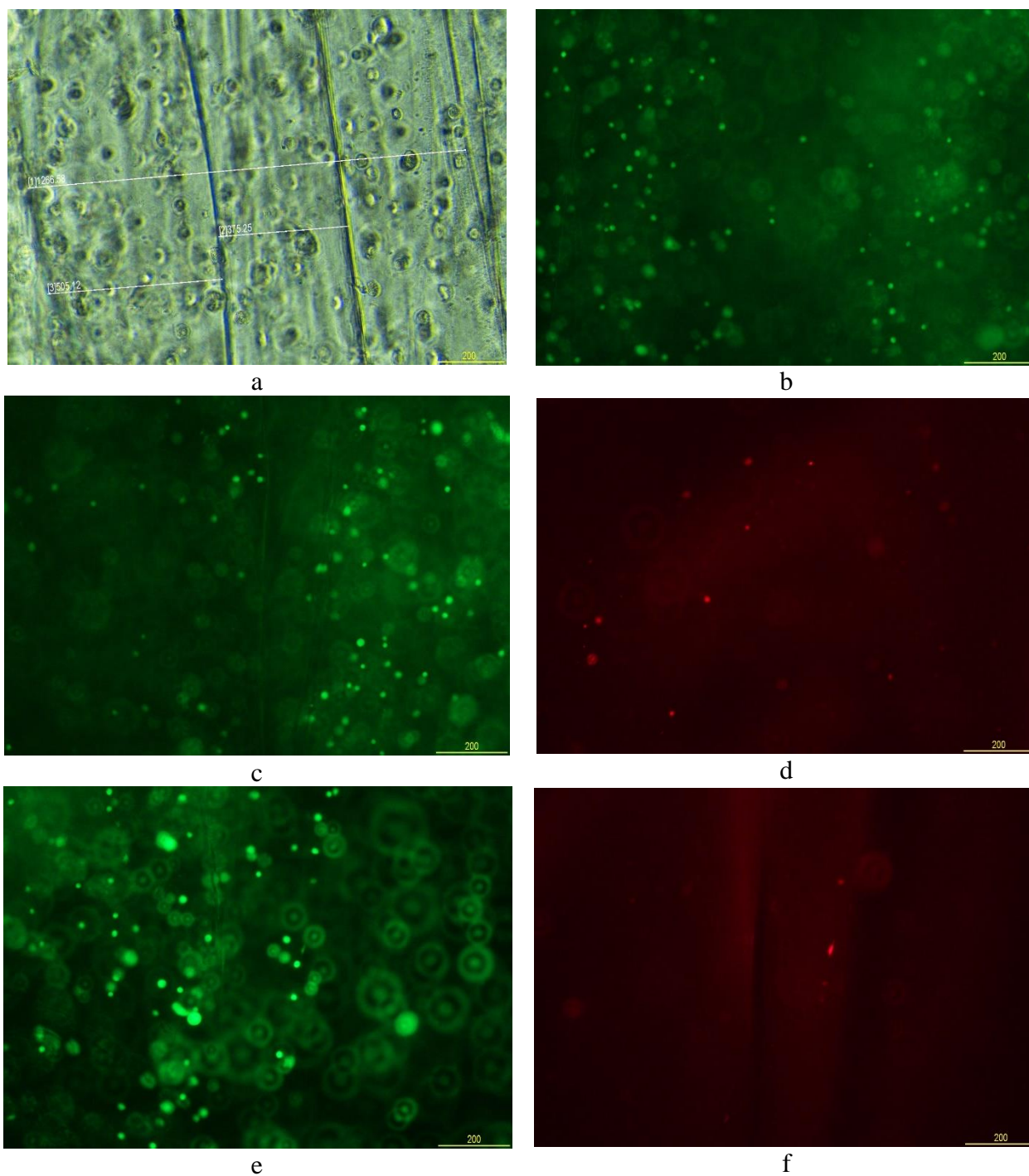


Figure 19: (a) Top surface view of the printed tubule in horizontal position, (b) Live cells on the printed tubule just after printing when the confocal microscope was focused on the mid surface level, and (c, d ,e, and f) live/dead assay on two different part of the same structure after 5 days of incubation

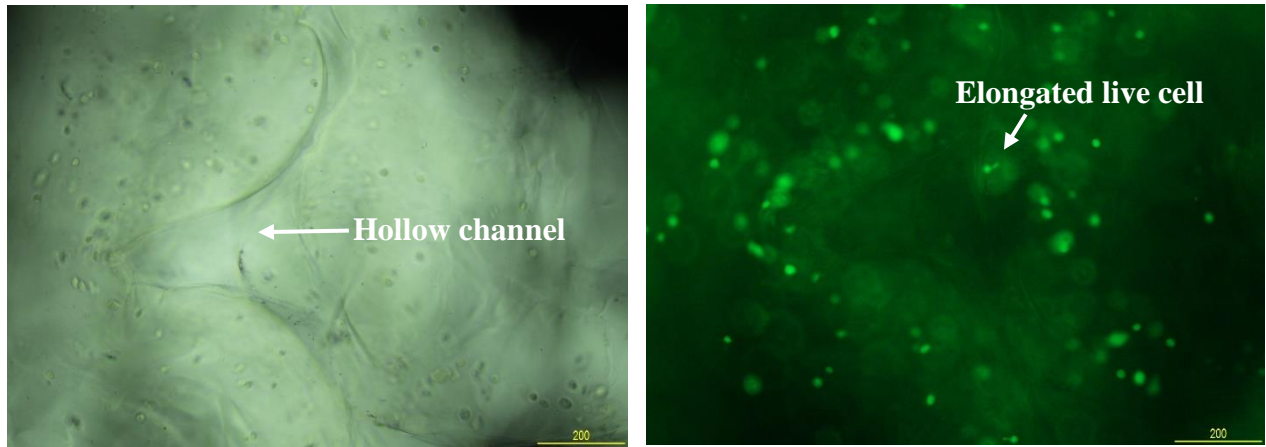


Figure 20: Cross sectional view of the printed structure and living cells after 5 days of incubation

Figure 20 shows the cross-sectional view of the cell-laden tubular structure. It shows that there is no defined circular channel inside the tubular structure. As the printed structure was submerged into the complete classic media, ionic diffusion could change the structure of the printed hydrogel. This could be a reason for the narrower channel. Another reason could be the nozzle clogging which may lead to the off-centered calcium chloride flow.

CHAPTER V

CONCLUSION

In this study, experimental studies are conducted to investigate the printability of tubular structure by co-axial extrusion bioprinting system. Optimal printing parameters are identified for the continuous and consistent production of a hollow tubular structure with proper dimensions. From the experimental results, it is concluded that the interaction of flow rate and alginate concentration has a significant effect on the tubule diameter and CaCl_2 concentration did not affect the tubule diameter in a distinct trend. However, from the optimization results, when the CaCl_2 concentration was more than 1.5 times alginate concentration, the tubular dimensions were more accurate with nozzle dimensions. For collagen-alginate bioink, the optimum alginate concentration was 1.7%. For pure alginate bioink, the optimum flow rate and alginate concentrations were 780 $\mu\text{l}/\text{min}$ and 2% respectively.

Finally, with these process parameters, the cell-laden tubular structure was printed with pure alginate. The cross-section was observed. From the cross-section, we did not get any defined channel diameter. As the printed structure was submerged in the media, it could be a reason to collapse the hydrogel structure. After 5 days of printing, the live/dead assay was observed with a confocal microscope. We found that though live cell % is higher, cell morphology was not noticeable. Very few cells were elongated as spindle shape which is

the original shape of the smooth muscle cell. For better cell morphology, in the future study, a protein-based bioink such as Collagen should be incorporated with alginate.

In the future study, triaxial nozzle will be used to print bilayer tubular structure where endothelial cells will be in the inner layer and smooth muscle cell will be in the outer layer. The future goal is to fabricate a functional smaller diameter bilayer blood vessel and observe the vasodilation and vasocontraction behavior

REFERENCES

- Axpe, E., & Oyen, M. L. (2016, Nov 25). Applications of Alginate-Based Bioinks in 3D Bioprinting. *Int J Mol Sci*, 17(12). <https://doi.org/10.3390/ijms17121976>
- Bacakova, L., Travnickova, M., Filova, E., Matějka, R., Stepanovska, J., Musilkova, J., Zarubova, J., & Molitor, M. (2018). The role of vascular smooth muscle cells in the physiology and pathophysiology of blood vessels. *Muscle Cell Tissue Curr. Status Res. Field*, 229.
- Banerjee, A., Arha, M., Choudhary, S., Ashton, R. S., Bhatia, S. R., Schaffer, D. V., & Kane, R. S. (2009). The influence of hydrogel modulus on the proliferation and differentiation of encapsulated neural stem cells. *Biomaterials*, 30(27), 4695-4699.
- Dickman, C. T. D., Russo, V., Thain, K., Pan, S., Beyer, S. T., Walus, K., Getsios, S., Mohamed, T., & Wadsworth, S. J. (2020, Jan). Functional characterization of 3D contractile smooth muscle tissues generated using a unique microfluidic 3D bioprinting technology. *FASEB J*, 34(1), 1652-1664. <https://doi.org/10.1096/fj.201901063RR>
- Ding, H., & Chang, R. (2018). Printability Study of Bioprinted Tubular Structures Using Liquid Hydrogel Precursors in a Support Bath. *Applied Sciences*, 8(3). <https://doi.org/10.3390/app8030403>
- Duan, B., Hockaday, L. A., Kang, K. H., & Butcher, J. T. (2013). 3D bioprinting of heterogeneous aortic valve conduits with alginate/gelatin hydrogels. *Journal of biomedical materials research Part A*, 101(5), 1255-1264.
- Gao, Q., He, Y., Fu, J. Z., Liu, A., & Ma, L. (2015, Aug). Coaxial nozzle-assisted 3D bioprinting with built-in microchannels for nutrients delivery. *Biomaterials*, 61, 203-215. <https://doi.org/10.1016/j.biomaterials.2015.05.031>
- Gombotz, W. R., & Wee, S. (1998). Protein release from alginate matrices. *Advanced drug delivery reviews*, 31(3), 267-285.
- Gu, Z., Fu, J., Lin, H., & He, Y. (2019). Development of 3D bioprinting: From printing methods to biomedical applications. *Asian Journal of Pharmaceutical Sciences*.

- Gu, Z., Fu, J., Lin, H., & He, Y. (2020, Sep). Development of 3D bioprinting: From printing methods to biomedical applications. *Asian J Pharm Sci*, 15(5), 529-557.
<https://doi.org/10.1016/j.aips.2019.11.003>
- Guillotin, B., & Guillemot, F. (2011). Cell patterning technologies for organotypic tissue fabrication. *Trends in biotechnology*, 29(4), 183-190.
- Gulrez, S. K. Saphwan Al-assaf, and Glyn O. Phillips. 2003. "Hydrogels: Methods of Preparation, Characterisation and Applications.". *Advanced Research*, 6(2), 105-121.
- Habib, A., Sathish, V., Mallik, S., & Khoda, B. (2018, Mar 20). 3D Printability of Alginate-Carboxymethyl Cellulose Hydrogel. *Materials (Basel)*, 11(3).
<https://doi.org/10.3390/ma11030454>
- Hospodiuk, M., Dey, M., Sosnoski, D., & Ozbolat, I. T. (2017). The bioink: A comprehensive review on bioprintable materials. *Biotechnology advances*, 35(2), 217-239.
- Langer, R. S., & Vacanti, J. P. (1999). Tissue engineering: the challenges ahead. *Scientific American*, 280(4), 86-89.
- Liu, W., Zhong, Z., Hu, N., Zhou, Y., Maggio, L., Miri, A. K., Fragasso, A., Jin, X., Khademhosseini, A., & Zhang, Y. S. (2018, Jan 12). Coaxial extrusion bioprinting of 3D microfibrous constructs with cell-favorable gelatin methacryloyl microenvironments. *Biofabrication*, 10(2), 024102. <https://doi.org/10.1088/1758-5090/aa9d44>
- Naghieh, S. (2020). *Extrusion bioprinting of hydrogel scaffolds: printability and mechanical behavior* [University of Saskatchewan].
- Naghieh, S., & Chen, D. (2021). Printability – a Key Issue in Extrusion-based Bioprinting. *Journal of Pharmaceutical Analysis*. <https://doi.org/10.1016/j.jpha.2021.02.001>
- Naghieh, S., Karamooz-Ravari, M. R., Sarker, M. D., Karki, E., & Chen, X. (2018, Apr). Influence of crosslinking on the mechanical behavior of 3D printed alginate scaffolds: Experimental and numerical approaches. *J Mech Behav Biomed Mater*, 80, 111-118.
<https://doi.org/10.1016/j.jmbbm.2018.01.034>
- Naghieh, S., Sarker, M., Sharma, N., Barhoumi, Z., & Chen, X. (2020). Printability of 3D printed hydrogel scaffolds: Influence of hydrogel composition and printing parameters. *Applied Sciences*, 10(1), 292.
- Novosel, E. C., Kleinhans, C., & Kluger, P. J. (2011, Apr 30). Vascularization is the key challenge in tissue engineering. *Adv Drug Deliv Rev*, 63(4-5), 300-311.
<https://doi.org/10.1016/j.addr.2011.03.004>

- Osidak, E. O., Kozhukhov, V. I., Osidak, M. S., & Domogatsky, S. P. (2020). Collagen as Bioink for Bioprinting: A Comprehensive Review. *Int J Bioprint*, 6(3), 270. <https://doi.org/10.18063/ijb.v6i3.270>
- Ozbolat, I. T., & Hospodiuk, M. (2016). Current advances and future perspectives in extrusion-based bioprinting. *Biomaterials*, 76, 321-343.
- Panchal, N., Patel, D., & Shah, N. Synthesis of Hydrogels.
- Reagan, A. M., Gu, X., Paudel, S., Ashpole, N. M., Zalles, M., Sonntag, W. E., Ungvari, Z., Csiszar, A., Otolara, L., & Freeman, W. M. (2018). Age-related focal loss of contractile vascular smooth muscle cells in retinal arterioles is accelerated by caveolin-1 deficiency. *Neurobiology of aging*, 71, 1-12.
- Tønnesen, H. H., & Karlsen, J. (2002). Alginate in drug delivery systems. *Drug development and industrial pharmacy*, 28(6), 621-630.
- Udofia, E. N., & Zhou, W. (2019). A guiding framework for microextrusion additive manufacturing. *Journal of Manufacturing Science and Engineering*, 141(5).
- Ullah, F., Othman, M. B. H., Javed, F., Ahmad, Z., & Akil, H. M. (2015). Classification, processing and application of hydrogels: A review. *Materials Science and Engineering: C*, 57, 414-433.
- Vafaei, S., Tuck, C., Ashcroft, I., & Wildman, R. (2016). Surface microstructuring to modify wettability for 3D printing of nano-filled inks. *Chemical Engineering Research and Design*, 109, 414-420.
- Włodarczyk-Biegun, M. K., & Del Campo, A. (2017). 3D bioprinting of structural proteins. *Biomaterials*, 134, 180-201.
- Xiao, L., Ding, M., Saadoon, O., Vess, E., Fernandez, A., Zhao, P., Jin, L., & Li, X. (2017). A novel culture platform for fast proliferation of human annulus fibrosus cells. *Cell and tissue research*, 367(2), 339-350.
- Xu, L., Varkey, M., Jorgensen, A., Ju, J., Jin, Q., Park, J. H., Fu, Y., Zhang, G., Ke, D., Zhao, W., Hou, R., & Atala, A. (2020, Jul 29). Bioprinting small diameter blood vessel constructs with an endothelial and smooth muscle cell bilayer in a single step. *Biofabrication*, 12(4), 045012. <https://doi.org/10.1088/1758-5090/aba2b6>
- Yang, X., Lu, Z., Wu, H., Li, W., Zheng, L., & Zhao, J. (2018, Feb 1). Collagen-alginate as bioink for three-dimensional (3D) cell printing based cartilage tissue engineering. *Mater Sci Eng C Mater Biol Appl*, 83, 195-201. <https://doi.org/10.1016/j.msec.2017.09.002>

Yeong, W. Y., Sudarmadji, N., Yu, H. Y., Chua, C. K., Leong, K. F., Venkatraman, S. S., Boey, Y. C., & Tan, L. P. (2010, Jun). Porous polycaprolactone scaffold for cardiac tissue engineering fabricated by selective laser sintering. *Acta Biomater*, 6(6), 2028-2034.
<https://doi.org/10.1016/j.actbio.2009.12.033>

BIOGRAPHICAL SKETCH

Taieba Tuba Rahman has acquired her bachelor's degree in Industrial and Production Engineering from Khulna University of Engineering and Technology, Bangladesh in 2014. After completing her undergraduate, she worked in the apparel industry as a system engineer for around 1 year. Then She served as a lecturer for around 3 years in an Engineering Institution. Taieba joined the department of Manufacturing and Industrial Engineering at the University of Texas Rio Grande Valley in August 2019 for pursuing her Master's. She worked as a research assistant under Dr. Jianzhi Li and completed her Master of Science in Manufacturing Engineering in August 2021. Her research interests are focused on Biofabrication and Additive manufacturing. During her Master's, she published one article titled "Analysis of the operating conditions of pulse electric field-assisted EHD for sodium alginate printing using design of experiment approach". She can be reached at taiebatuba@gmail.com.